the different recombinant bacteria during different sol–gel preparation protocols will be presented elsewhere.

Our experiments point to the high biocompatibility of recombinant *E. coli* to sol–gel derived silicate gels, as indicated by two independent observations: 1) The encapsulated bacteria maintain their physiological ability to synthesize a fully functional luciferase and sufficient substrate to generate luminescence. This ability was maintained even after 4 weeks of storage, with a very similar dose-dependency to that of non-encapsulated cells. 2) The silicate cages do not significantly induce heat shock, emergency (SOS) DNA damage repair, and anti-peroxide protective systems of the bacterial strains during prolonged storage. It has been previously shown that these systems are very sensitive indicators of the well-being of the cells as well as of the integrity of their genetic material. The fact that they were not induced to luminesce is indicative of the benign nature of the encapsulation state. It is worth noting, however, that the caging process, either by methanol generation or due to physical caging, did temporarily induce heat-shock and genotoxicity stress conditions, manifested by transient luminescence during the first several hours of gel formation.

Experimental

Bacterial Strains: *E. coli* strains TV1061, DPD2794, and DPD2511 were prepared according to the procedures outlined by Van Dyk et al. [11], Vollmer et al. [12], and Belkin et al. [13], respectively.

Preparation of Bacteria: Prior to encapsulation, the bacterial strains were grown overnight (37 °C, with shaking) in LB broth, containing 100 μg/mL ampicilin to ensure plasmid maintenance. The culture was then diluted 100-fold with fresh LB and regrown under the same conditions to a density of about 10^8 cells/mL (20 klett units, about 0.2 OD at 600 nm). For measurement of the effect of the different inducers on the luminescence response of suspended bacteria, early exponential growth cultures were exposed to the inducer in an opaque white microtiter plate (Costar Europe, Bdhoevedrop, The Netherlands). The plates were incubated at 25 °C and luminescence was measured by a microtiter plate luminescence detector (Victor^2, EG&G Wallac, Turku, Finland). LB and bacterial suspension without inducers served as controls. Luminescence response of the encapsulated bacteria was measured by a similar procedure with the exception that the wet bacteria encapsulated plate was placed in the microtiter plate well containing 100 μL LB solution with the set level of the inducer.

Encapsulation Procedure: The sol–gel plates were prepared by mixing 4 mL of tetramethylorthosilicate (Aldrich) with 2 mL of distilled water and 0.5 mL of 0.1 M HCl. The mixture was sonicated for 10 min to ensure uniformity and left at 4 °C for a day. 3 mL of the *E. coli* suspension (10^8 cells/mL) in LB was mixed with 0.5 mL of the sol–gel solution, then a set amount of the mixture was deposited on a 4 × 4 mm glass plate and partly dried for 5 min under ambient conditions. After partial drying, the *E. coli*–sol–gel film was washed with a phosphate buffer (pH 7), and kept in the microtiter plate wells. The thickness of the sol–gel coating was approximately 1 mm, as measured by optical microscopy.

Received: May 21, 2001

[1] S. Kohler, T. T. Bachmann, J. Schmitt, S. Belkin, R. D. Schmid, *Sens. Actuators B* **2000**, *70*, 139.
[2] S. Daunert, G. Barrett, J. S. Feliciano, R. S. Shetty, S. Shrestha, W. Smith-Spencer, *Chem. Rev.* **2000**, *100*, 2705.
[3] D. Avnir, *Accounts Chem. Res.* **1995**, *28*, 328.
[4] D. Avnir, S. Braun, O. Lev, M. Ottolenghi, *Chem Mater.* **1994**, *6*, 1605.
[5] B. C. Dave, B. Dunn, J. S. Valentine, J. I. Zink, *Anal. Chem*. **1994**, *66*, 1120.
[6] S. Y. Chia, J. Urano, F. Tamanoi, B. Dunn, J. I. Zink, *J. Am. Chem. Soc.* **2000**, *122*, 6488.
[7] E. A. Pope, K. Braun, C. M. Peterson, *J. Sol-Gel Sci. Technol.* **1997**, *8*, 635.
[8] T. Branyik, G. Kuncova, J. Paca, K. J. Demnerova, *J. Sol-Gel Sci. Technol.* **1998**, *13*, 283.
[9] L. Inama, S. Dire, G. Carturan, A. Cavazza, *J. Biotechnol.* **1993**, *30*, 197.
[10] S. Fennough, S. Guyou, J. Livage, C. Rouse, *J. Sol-Gel Sci. Technol.* **2000**, *19*, 647.
[11] T. K. Van Dyk. W. R. Majarian, K. B. Konstantinov, R. M. Young, P. S. Dhurjati, R. A. La Rossa, *Appl. Environ. Microbiol*. **1994**, *60*, 1414.
[12] A. C. Vollmer, S. Belkin, D. R. Smulski, T. K. Van Dyk, R. A. La Rossa, *Appl. Environ. Microbiol*. **1997**, *63*, 2566.
[13] S. Belkin, D. R. Smulski, A. C. Vollmer, T. K. Van Dyk, R. A. La Rossa, *Appl. Environ. Microbiol.* **1996**, *62*, 225.

Poly(naphthodithiophene)s: Robust, Conductive Electrochromics via Tandem Cyclization–Polymerizations**

By *John D. Tovar* and *Timothy M. Swager**

Due to the high stability of conducting polythiophenes, extensive efforts have targeted new thiophene architectures that allow for enhanced materials properties, easier processing, and higher stability.[1] For example, rigidly enforcing planarity between conjugated thienyl centers can decrease optical bandgaps of the resulting polymer due to more effective π-overlap.[2] In search of highly stable electrochromic materials, we have become interested in the incorporation of polycyclic aromatic residues into a conjugated polymer backbone. While Bard has used this strategy to impart greater stability into electrochromic carbonoid ladder polymers,[3] we sought to include thiophene-based polycyclic aromatics for further enhancement of stability. To effectively synthesize such materials, we describe herein a tandem cyclization–polymerization scheme to produce aromatized monomers in situ prior to oxidative polymerization. Within this context, Scheme 1 depicts such a sequence where a generic pendant thienyl monomer undergoes an oxidative cyclization to provide an aromatized material containing a bithiophene repeat unit planarized by a bridging benzeno segment.[4] The a priori regularity afforded by the symmetry of these fused monomers eliminates any regiochemical "head-to-tail" coupling issues during polymerization,[5] allowing for a greater degree of coplanarity between repeat units and hence, enhanced conductivity within these new materials. From another standpoint, the topological similarity of the fused monomers to triphenylene offers an opportunity to utilize this discotic organizational element in the design of new liquid crystalline[6] or electronic materials.[7] Introducing fused thiophene moieties simplifies synthetic manipulation relative to triphenylene cores, thus enabling greater flexibility to fine-tune a desired molecular property. In this

[*] Prof. T. M. Swager, J. D. Tovar
Department of Chemistry, Massachusetts Institute of Technology
77 Massachusetts Avenue, Cambridge, MA 02139 (USA)
E-mail: tswager@mit.edu

[**] We appreciate financial support from the ARO (TOPS-MURI). We thank D. J. Mascaro and T. McClure (MIT Department of Materials Science and Engineering) for assistance with conductivity measurements and H.-H. Yu and Dr. A. E. Pullen for helpful discussions. T. M. Long, Dr. H. E. Bronstein, and Dr. Q. Zhou generously supplied precursor materials to **1a–b** and α-**1**. The NSF provided funding for the Department of Chemistry Instrumentation Facility (DCIF) and the Center for Materials Science and Engineering (CMSE) Shared Facility.

  0935-9648/01/2312-1775 $ 17.50+.50/0

ADVANCED MATERIALS

regard, we discuss spectroelectrochemical data that demonstrates the significant electronic differences available through facile structural modifications of the precursor monomers.

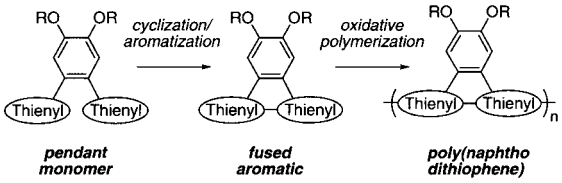

Scheme 1.

From readily available halogenated arenes, Suzuki coupling with 3-thiophene boronic acid provided multigram quantities of the β-thienyl redoxophores **1** in high yield,[8] while Stille coupling with 2-tributylstannyl thiophene provided the α-thienyl α-**1** isomer (Scheme 2).[9] Cyclic voltammetry (CV) of **1a** (Fig. 1A; 0.27 mM) and α-**1** (Fig. 1C; 1.72 mM) revealed two distinct and irreversible monomer oxidation peaks as the only anodic signals present in the first oxidative scan (0.83 and 0.91 V for **1a**; 0.87 and ca. 1.07 V for α-**1**). Subsequent voltammetric sweeps revealed the growth of low potential polymer-based redox activity that increased with additional scanning (see also Fig. 1D and F). Deposition required successive cycling to the most positive monomer oxidation potential as no polymer film growth occurred at applied potentials below 0.90 V. From these data, we propose the two major mechanistic steps illustrated in Scheme 2 for both isomers. Specifically, after electrochemical oxidation of a pendant thienyl moiety of **1**, an intramolecular α–α cyclization and deprotonation provides the aromatized naphthodithiophene **2**.[10] Further oxidation of **2** at higher potential ultimately leads to polymer growth through the remaining α' sites. In an analogous fashion, oxidation of α-**1** leads to the isomeric aromatized monomer by way of a β–β cyclization followed by higher potential polymerization through the vacant α sites to provide poly(α-**2**).[11]

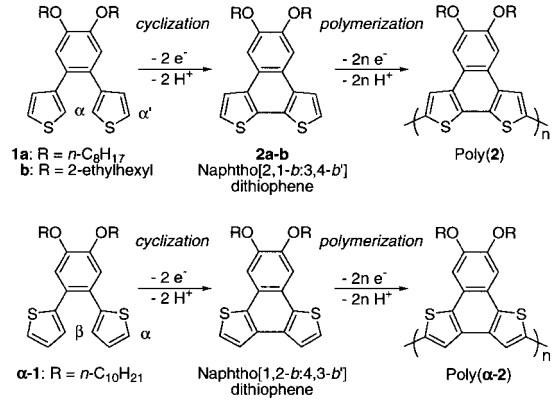

Scheme 2.

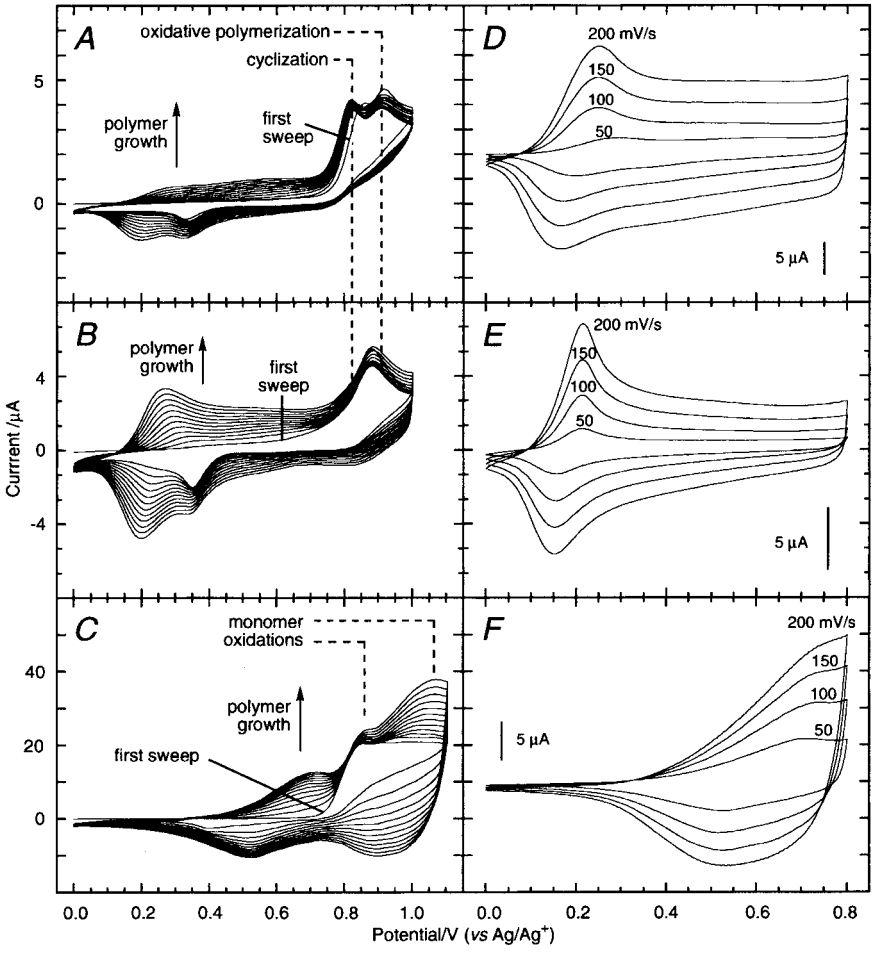

Fig. 1. Monomer (A, B, and C) and polymer (D, E, and F) CV: **1a** (A; 0.27 mM), **2a** (B; sat. ca. 0.3 mM), leading to poly(**2**) (D and E) and α-**1** (C; 1.72 mM) leading to poly(α-**2**) (F) at a 2 mm^2 Pt button electrode in 0.1 M n-Bu_4PF_6 (CH_3CN). Monomer CVs cycled at 100 mV/s; polymer film CVs obtained at 50–200 mV/s $E_{1/2}$(Fc/Fc$^+$): +0.086 V.

  0935-9648/01/2312-1776 $ 17.50+.50/0

To support our mechanism (Scheme 2), we synthesized intermediate **2** by using $FeCl_3$ as an oxidant.[12] In the presence of vacant β sites on the thienyl rings, we anticipated that the two different α sites of **1** would exhibit the most chemical and electrochemical reactivity (labeled α and α' in Scheme 2). As such, we sought to independently address the first step of the polymerization (the α–α coupling). While $FeCl_3$ has served as a suitable chemical oxidant during polythiophene synthesis, we could minimize undesired polymerization of **1** through use of short reaction times with near-stoichiometric amounts of oxidant. We subjected a saturated solution of sparingly soluble **2** to the same electropolymerization conditions as monomer **1** and obtained the representative deposition growth in Figure 1B (ca. 0.3 mM). Note that the first sweep displayed only one monomer oxidation peak at 0.88 V that corresponded to the second monomer oxidation displayed by **1** (Fig. 1A), and all subsequent sweeps displayed similar polymer-based redox activity centered at lower potential (see also Fig. 1E). The close resemblance of the polymer films obtained from **1** and from **2** (Fig. 1D and E, respectively) supports the fact that the deposited materials have the same structural connectivity although the typically poor solubility and trace amounts of electrochemically deposited material prevented more rigorous structural characterization (vide infra). The CVs for poly(**2**) exhibit reversible electroactivity over a broad range of potentials consistent with a highly delocalized system (Fig. 1D,E). In contrast, poly(α-**2**) requires higher potentials for electroactivity and displays less reversible behavior (Fig. 1F). Attempts to obtain in situ conductivites did not succeed due to poor adhesion of uniform polymer films on interdigitated microelectrodes, so we could not make a direct comparison of conductivity between poly(**2**) and poly(α-**2**). However, the sluggish electrochemical kinetics, the higher oxidation potential, and the larger optical band gap observed for poly(α-**2**) indicate that this material has a more localized electronic structure and a lower conductivity (Fig. 1F, vide infra).

The differing degrees of backbone delocalization available to poly(**2**) and isomeric poly(α-**2**) manifest themselves upon inspection of the spectroelectrochemistry presented in Figure 2. Electrodeposition on transparent In–SnO_2 glass electrodes of red poly(**2**) films and yellow poly(α-**2**) films (from **1a** and α-**1**, respectively) provided films that transformed to dark blue as the anodic potential cycled through values sufficiently high to oxidize the polymer. Attesting to the extraordinary stability imparted by the naphthodithiophene moieties, the electroactivity and electrochromicity of these films persisted after over 10 000 scans under ambient atmospheric conditions. Poly(**2**) displayed a low energy absorption centered at 620 nm along with a near-infrared (NIR) absorbance that increased with further oxidation (Fig. 2, top). For poly(α-**2**), a low energy band centered at 550 nm appeared with increased oxidation along with a broad NIR band that drifted to higher energy with further doping (Fig. 2, middle). The well-defined higher energy transition coupled with this NIR drift implies that poly(α-**2**) has a more localized electronic structure than

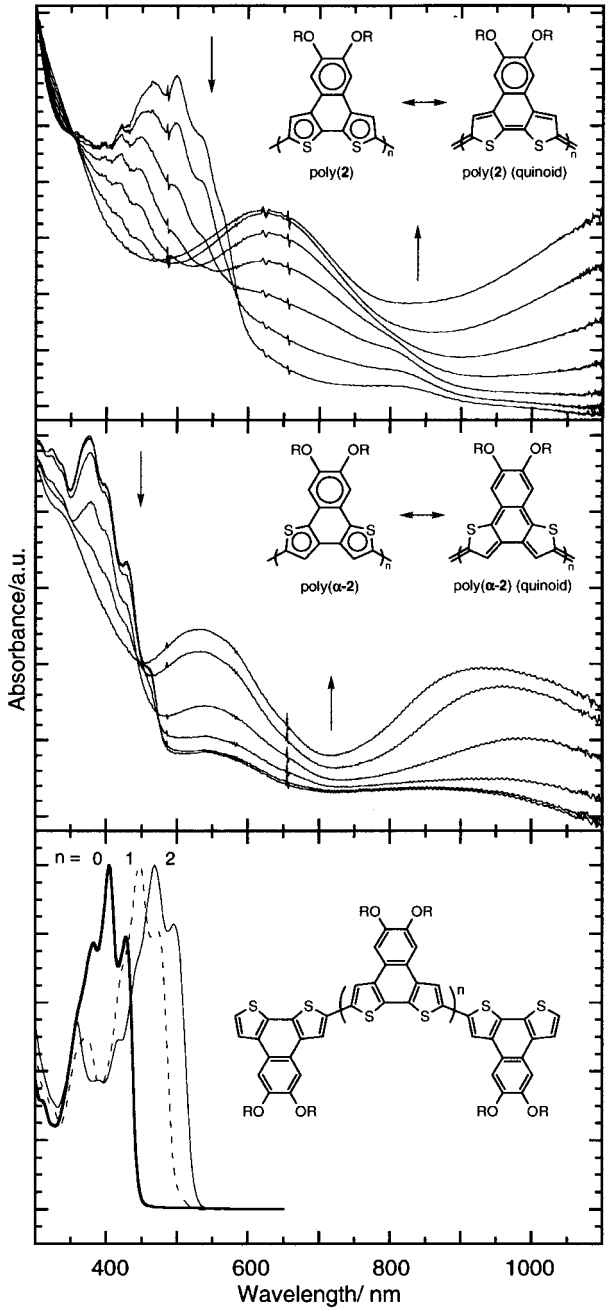

Fig. 2. Changes in UV-vis absorption upon increased oxidation for films of poly(**2**) (top) and poly(α-**2**) (middle) grown on ITO-coated electrodes and held at ca. 120 mV steps between 0.15–0.90 V. Other conditions as in Figure 1. For comparison, the bottom spectrum shows the absorptions (from GPC eluents) for a series of oligo(**2**)s in THF: dimer (bold), trimer (- - - -), and tetramer (—).

that of poly(**2**). After considering the quinoidal polymer resonance structures (Fig. 2, insets), poly(α-**2**) should possess a low degree of electronic delocalization due to the necessary disruption of aromaticity within the fused benzo fragment of the repeat unit. Indeed, the higher oxidation potential and ultraviolet-visible (UV-vis) absorbances of poly(α-**2**) reflect the energetic cost of delocalizing charge within the oxidized material. From this argument, it follows that poly(**2**) oxidizes at

  0935-9648/01/2312-1777 $ 17.50+.50/0

ADVANCED MATERIALS

lower potential due to the extended thiophene-centered quinoidal delocalization available without requiring significant aromatic perturbation in the benzo fragment. The relative energies of such quinoidal resonance contributions play important roles in determining the band gaps of conjugated polymers.[13]

Electrochemically synthesized polythiophenes can have poor regiochemical integrity; namely, defects arising from head-to-tail scrambling and from β linkages will significantly affect the bulk properties of the polymer. To evaluate the selectivity of our chemistry, we performed bulk electrolyses on the 2-ethylhexyl derivatives **1b** and **2b**. Chronocoulometry indicated that the conversion of **1b** to **2b** consumed 2.1 e^-/mol at 0.85 V to provide a 75 % isolated yield of **2b**. Holding solutions of **1b** at 0.90–1.20 V provided a doubly cyclized dimer (n = 0 in Fig. 2, bottom) alongside higher oligomers and polymers. Likewise, subjecting **2b** to a 0.90 V potential yielded trace yet spectroscopically useful amounts of trimeric and tetrameric materials (n = 1, 2 of Fig. 2, bottom) again along with higher insoluble materials that prohibited gel permeation chromatography (GPC) analysis. UV-vis analysis of the GPC eluents reflected the oligomeric nature of the tetrahydrofuran (THF)-soluble materials as evidenced by the similarly structured yet increasingly lower energy λ_{max} absorptions corresponding to dimeric (404 nm), trimeric (448 nm), and tetrameric (468 nm) oligo(**2**)s shown in Figure 2 (bottom). The eluted GPC fractions of THF soluble oligomers derived either from bulk electrolysis or chemical oxidation of pendant monomer **1b** displayed comparable UV-vis absorptions to materials derived from **2b**, thus serving to further establish the tandem cyclization–polymerization reactivity.

In parallel, we have investigated the chemical functionalization of the highly soluble parent monomer core **2b**. For example, lithiation of **2b** ultimately led to the diiodide **3** in high yield (Scheme 3). To further verify the structural connectivity of electrochemically prepared poly(**2**), we used Kelly's in situ stannylation/cross-coupling strategy to obtain regiochemically well-defined poly(**2**) from **3**.[14] As with bulk electrochemical polymerization, we obtained insoluble materials that precipitated during the course of the reaction, apparently a result of aggregation between the naphthodithiophene repeat units. However, sufficient amounts of the polymer dissolved in hot *o*-dichlorobenzene to allow for the preparation of dark red drop-cast films suitable for four-point probe conductivity determination. Taken in ambient atmosphere, these measurements revealed a conductivity of 1.3 S/cm with saturative doping by iodine vapor. These chemically cross-coupled materials resembled the electrochemically synthesized poly(**2**)s: cross-coupled poly(**2**) absorbed strongly at 487, 518, and 566 nm (in $CHCl_3$), and neutral poly(**2**) anodically deposited on In–SnO_2 absorbed at 464 and 498 nm with shoulders at 533 and 562 nm (Fig. 2, top). In line with the oxidatively derived material, UV-vis analysis of the GPC eluents for THF soluble, cross-coupled oligo(**2**) showed a similar λ_{max} progression to lower energies for the dimer (412 nm), trimer (452 nm), and tetramer (476 nm).

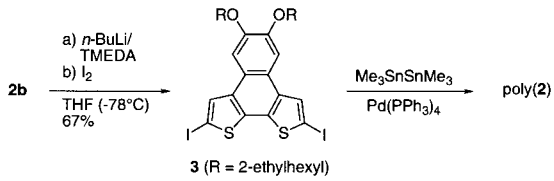

Scheme 3.

In summary, we have designed and synthesized a series of polyaromatic monomers that display excellent chemical and electrochemical behavior. The pendant thienyls **1** and α-**1** undergo a tandem cyclization–polymerization process to yield a new class of robust electrochromic materials. To further study this process, we developed efficient chemical and electrochemical syntheses of the naphtho[2,1-*b*:3,4-*b*′]dithiophene core **2**, a monomer poised for further investigation. In analogy to the iodination/cross-coupling route to poly(**2**), preliminary work has shown that Suzuki, Stille, and Sonogashira[15] protocols can also provide easy access to a variety of extended monomeric systems. Through judicious choices of pendant functionality, we plan to tune the liquid crystallinity and electroactivity of these systems. Ongoing efforts in our laboratories center on utilizing this chemistry for syntheses of larger monomers for subsequent incorporation into novel organic materials.

Experimental

General: Methylene chloride, THF, and tetramethylethylenediamine (TMEDA), were passed through activated alumina columns prior to use and TMEDA was then distilled from KOH; *n*-BuLi in hexane was titrated versus diphenylacetic acid before use. All other chemicals were of reagent grade and used as received. Air and water sensitive reactions employed standard Schlenk techniques under argon atmosphere. Nuclear magnetic resonance (NMR) chemical shifts are referenced to residual $CHCl_3$ (7.26 ppm for ^{1}H, 77.23 ppm for ^{13}C) or $CHDCl_2$ (5.32 ppm for ^{1}H, 54.00 ppm for ^{13}C); aromatic carbon multiplicities were determined by distortionless enhancement by polarization transfer (DEPT) analysis. Conductivity measurements were determined by the four-point probe method; film thicknesses were determined on surface profiler.

Electrochemistry: All electrochemical measurements were made with an Autolab PGSTAT 20 potentiostat (Eco Chemie). CV was performed in oven-dried, argon-purged one chamber three electrode cells versus a quasi-internal Ag wire reference electrode (BioAnalytical Systems) submersed in 0.01 M $AgNO_3$/0.1 M *n*-Bu_4NPF_6 in anhydrous MeCN. Spectroelectrochemistry was performed under ambient laboratory conditions on polymer films electrodeposited onto indium tin oxide (ITO) coated glass electrodes. The films were placed in a quartz cuvette in the path of the light source along with counter and reference electrodes as used above. The film was allowed to equilibrate for 30 s at a given oxidation potential prior to measuring the absorption spectrum. Bulk electrolyses were conducted vs. Ag/Ag^+ at a ca. 4 cm^2 Pt gauze electrode in a 2 chambered cell separated by a glass frit to allow for isolation of the Pt gauze (ca. 6 cm^2) counterelectrode.

*4,5-Bis(3-thienyl)-1,2-dioctyloxybenzene (**1a**)*: A three-necked 1 L flask was charged with 1,2-dibromo-4,5-dioctyloxybenzene [16] (8.74 g, 17.75 mmol), 3-thiophene boronic acid (5.00 g, 39.07 mmol), Na_2CO_3 (15.01 g, 141.6 mmol) and equipped with a condenser. Toluene (285 mL), EtOH (70 mL), and H_2O (70 mL) were added to the flask and the solution was vigorously stirred during a 1 h purge with argon. Under a gentle argon stream, $Pd(PPh_3)_4$ (605 mg, 0.524 mmol) was added to the solution and the system was heated at reflux for 18 h, cooled to room temperature and diluted with ether. After removing the aqueous layer, the organics were washed with 2 M KOH (×2), and NaCl (aq), and the organic phase was dried ($MgSO_4$) and removed in vacuo. Chromatography of the crude material on silica gel (3:1 hexane/CH_2Cl_2) provided the product as a chaulky white solid (8.330 g, 16.70 mmol, 94 %). Melting point (m.p.) 74–75 °C. ^{1}H NMR (300 MHz, $CDCl_3$) δ: 7.17 (dd, 2H, J = 3.0, 4.8 Hz), 7.01

  0935-9648/01/2312-1778 $ 17.50+.50/0

(dd, 2H, J = 1.2, 3.0 Hz), 6.96 (s, 2H), 6.78 (dd, 2H, J = 1.05, 4.95 Hz), 4.05 (t, 4H, J = 6.6 Hz), 1.85 (quin, 4H, J = 6.9 Hz), 1.49 (m, 4H), 1.30 (bm, 16H), 0.90 (t, 6H, J = 6.3 Hz). ^{13}C NMR (100 MHz, $CDCl_3$) δ: 148.5, 142.2, 129.3, 128.1, 124.7, 122.5, 115.9, 69.6, 32.0, 29.57, 29.50 (2C), 26.2, 22.9, 14.3. Fourier transform infrared spectroscopy (FTIR) (KBr): ν/cm^{-1}: 3096, 2954, 2921, 2852, 1602, 1536, 1505, 1467, 1386, 1259, 1163, 1060, 781, 676. UV-vis ($CHCl_3$) λ/nm (logε): 241 (4.29), 279 (3.94). High-resolution mass spectrometry (HR-MS) (electron impact, EI): found m/z = 498.2617 ± 0.0015 (M^+); calc. for $C_{30}H_{42}O_2S_2$: 498.2626.

*1,2-Bis(2′-ethylhexyloxy)-4,5-bis(3-thienyl)benzene (**1b**)*: Following the procedure for **1a** except for the use of 4,5-bis(2′-ethylhexyloxy)-1,2-dibromobenzene [17] (4.93 g, 10.01 mmol) and a reaction time of 45 h, chromatography of the crude material on silica gel (hexane to 3:1 hexane/CH_2Cl_2) provided the product as a viscous, opaque white oil (4.068 g, 8.16 mmol, 82 %). ^{1}H NMR (400 MHz, $CDCl_3$) δ: 7.17 (dd, 2H, J = 3.0, 4.89 Hz), 7.02 (m, 2H, apparent dd), 6.95 (s, 2H), 6.79 (dd, 2H, J = 0.78, 4.96 Hz), 3.92 (m, 4H), 1.79 (m, 2H), 1.31–1.54 (bm, 16H), 0.93 (m, 12H). ^{13}C NMR (100 MHz, $CDCl_3$) δ: 149.0, 142.4, 129.3, 128.0, 124.7, 122.4, 115.6, 72.0, 39.8, 30.8, 29.3, 24.2, 23.3, 14.3, 11.4. FTIR (neat): ν/cm^{-1}: 3101, 2958, 2927, 2871, 1614, 1542, 1500, 1465, 1256, 1161, 1032, 846, 780. UV-vis (CH_2Cl_2) λ/nm (logε): 231 (4.49), 278 (4.11). HR-MS (EI): found m/z = 498.2615 ± 0.0014 (M^+); calc. for $C_{30}H_{42}O_2S_2$: 498.2626.

*4,5-Bis(3-thienyl)-1,2-didecyloxybenzene (α-**1**)*: A 25 mL Schlenk tube was charged with 4,5-didecyloxy-1,2-diiodobenzene [18] (0.999 g, 1.55 mmol) and $(Ph_3P)_2PdCl_2$ (51 mg, 0.073 mmol) and placed under argon. Degassed toluene (1 mL) and dimethylformamide (DMF) (3 mL) were added and the system was heated to 80 °C. 2-(Tributylstannyl)thiophene (1.3 mL, 3.89 mmol) was added dropwise, and the reaction was stirred at 80 °C for 6 h. After cooling, the mixture was pushed through a silica gel plug (hexane/CH_2Cl_2 1:1) and the solvents were removed. The crude material was dissolved in ether and washed with NH_4Cl, 1 M HCl, NaF (×2), and NH_4Cl (×2). The organic phase was dried ($MgSO_4$) and removed in vacuo to provide a yellow solid. Recrystallization from $CHCl_3$/MeOH provided the product as a chaulky white solid (733 mg, 1.32 mmol, 85 %). M.p. 68.5–69 °C. ^{1}H NMR (500 MHz, $CDCl_3$) δ: 7.22 (d, 2H, J = 6.0 Hz), 6.99 (s, 2H), 6.93 (m, 2H), 6.83 (d, 2H, J = 3.0 Hz), 4.04 (t, 4H, J = 6.5 Hz), 1.84 (quin, 4H, J = 7.0 Hz), 1.47 (quin, 4H, J = 7.0 Hz), 1.28 (m, 28H), 0.88 (t, 6H, J = 7.0 Hz). ^{13}C NMR (125 MHz, $CDCl_3$) δ: 148.79, 143.13, 126.99, 126.88, 126.49, 125.63, 116.32, 69.57, 32.14, 29.85, 29.80, 29.62, 29.57, 29.43, 26.23, 22.91, 14.36. FTIR (KBr): ν/cm^{-1}: 2955, 2919, 2850, 1600, 1504, 1467, 1260, 1233, 1160, 1074, 857, 692. UV-vis ($CHCl_3$) λ/nm (logε): 241 (4.27), 296 (4.24). HR-MS (EI): found m/z = 554.3243 ± 0.0016 (M^+); calc. for $C_{34}H_{50}O_2S_2$: 554.3252.

*5,6-Dioctyloxynaphtho[2,1-b:3,4-b′]dithiophene (**2a**)*: A solution of **1a** (330 mg, 0.662 mmol) in CH_2Cl_2 (15 mL) was stirred vigorously under argon as a suspension of $FeCl_3$ (450 mg, 2.77 mmol) in $MeNO_2$ (7 mL) was added dropwise [12]. The solution was stirred under an argon purge for 30 min at which point anhydrous MeOH was added and stirred for 30 min. The solvents were removed, and the residue was taken up in CH_2Cl_2 and stirred vigorously with NH_4OH (aq). The aqueous layer was washed twice with CH_2Cl_2, and the combined organics were washed with NH_4OH and NH_4Cl, dried and removed. Purification on silica (hexane to 4:1 hexane/CH_2Cl_2) provided the product as very faint yellow solid (216 mg, 0.4348 mmol, 66 %). M.p. 118.5–121 °C. ^{1}H NMR (400 MHz, $CDCl_3$) δ: 7.87 (d, 2H, J = 5.37 Hz), 7.69 (s, 2H), 7.46 (d, 2H, J = 5.34 Hz), 4.20 (m, 4H), 1.95 (m, 2H), 1.56 (m, 4H), 1.32 (bm, 16H), 0.91 (t, 6H, J = 6.54 Hz), 0.94 (t, 6H, J = 7.14 Hz). ^{13}C NMR (100 MHz, $CDCl_3$) δ: 149.0, 134.1, 130.6, 123.6, 122.90, 122.74, 106.9, 69.4, 32.1, 29.7, 29.53, 29.49, 26.3, 22.9, 14.4. FTIR (KBr): ν/cm^{-1}: 2953, 2925, 2851, 1618, 1517, 1467, 1391, 1252, 1181, 1108, 1069, 840, 728. UV-vis ($CHCl_3$) λ/nm (logε): 262 (4.58), 311 (3.80), 321 (3.84), 333 (3.75), 350 (3.75). HR-MS (ESI): found m/z = 519.2384 [(M+Na)$^+$]; calc. for $C_{30}H_{40}O_2S_2$+Na: 519.2362.

*5,6-Bis(2′-ethylhexyloxy)naphtho[2,1-b:3,4-b′]dithiophene (**2b**)*: Subjecting **1b** (504 mg, 1.01 mmol) to the same procedure as described for **2a** above, the crude mixture was pushed through a plug of silica. The eluent was concentrated and added dropwise to MeOH. After filtering off the precipitated yellow solids, the filtrate was evaporated and the crude product purified on silica gel (hexane to to 8:1 hexane/CH_2Cl_2) to provide the product as a faint yellow oil (272 mg, 0.548 mmol, 54 %) alongside the previously precipitated, doubly cyclized dimer (94 mg, 0.0948 mmol, 19 %) and higher oligomers. ^{1}H NMR (400 MHz, $CDCl_3$) δ: 7.89 (d, 2H, J = 5.38 Hz), 7.69 (s, 2H), 7.47 (d, 2H, J = 5.34 Hz), 4.09 (m, 4H), 1.89 (m, 2H), 1.37–1.62 (m, 16H), 1.01 (t, 6H, J = 7.49 Hz), 0.94 (t, 6H, J = 7.14 Hz). ^{13}C NMR (125 MHz, $CDCl_3$) δ: 149.3, 134.1, 130.4, 123.5, 122.76, 122.74, 106.4, 71.6, 39.8, 30.9, 29.4, 24.25, 24.23, 23.3, 14.4, 11.5. FTIR (neat): ν/cm^{-1}: 3101, 3072, 2957, 2927, 2871, 1619, 1515, 1448, 1380, 1252, 1190, 1107, 1017, 839, 720, 641. UV-vis (CH_2Cl_2) λ/nm (logε): 228 (4.43), 263 (4.81), 310 (4.00), 321 (4.04), 334 (3.93), 350 (3.96). HR-MS (EI): found m/z = 496.2458 ± 0.0014 (M^+); calc. for $C_{30}H_{40}O_2S_2$: 496.2470.

*5,6-Bis(2′-ethylhexyloxy)-2,9-diiodonaphtho[2,1-b:3,4-b′]dithiophene (**3**)*: A dry 100 mL Schlenk flask containing a solution of TMEDA (0.8 mL, 5.30 mmol) in 40 mL THF was cooled to –78 °C followed by the addition of 2.30 mL n-BuLi in hexanes (1.577 M, 3.627 mmol). The solution was stirred for 5 min, at which point a solution of **2b** (595 mg, 1.198 mmol) in 5 mL THF was added dropwise. After being held for 30 min at –78 °C, a solution of I_2 (2.18 g, 8.59 mmol) in 5 mL THF was added. After addition, the reaction was stirred from –78 °C to 25 °C over 5 h. 2 M KOH was added to quench the reaction and stirred overnight. The aqueous phase was washed with ether, and the combined organics were washed further with NH_4Cl (aq) and water. After drying ($MgSO_4$) and removing the solvent in vacuo, the pale yellow solid was dissolved in minimal CH_2Cl_2 and precipitated into MeOH. The collected solids were then recrystallized from $CHCl_3$/MeOH to provide the product as a fluffy pale yellow solid (603 mg, 0.8055 mmol, 67 %). M.p. 154.5–155 °C. ^{1}H NMR (400 MHz, $CDCl_3$) δ: 7.89 (s, 2H), 7.41 (s, 2H), 4.05 (m, 4H), 1.90 (m, 2H), 1.40–1.60 (bm, 16H), 1.01 (t, 6H, J = 7.38 Hz), 0.95 (t, 6H, J = 6.73 Hz). ^{13}C NMR (100 MHz, $CDCl_3$) δ: 149.7, 135.0, 133.9, 132.5, 121.2, 105.7, 74.0, 71.6, 39.8, 30.9, 29.4, 24.3, 23.3, 14.4, 11.5. FTIR (KBr): ν/cm^{-1}: 2957, 2925, 2857, 1617, 1519, 1447, 1380, 1259, 1189, 1084, 822. UV-vis ($CHCl_3$) λ/nm (logε): 267 (4.61), 335 (4.14), 350 (4.12). HR-MS (EI): found m/z = 748.0372 (M^+); calc. for $C_{30}H_{38}I_2O_2S_2$: 748.0397.

*Poly(**2**): (Representative Procedure from **1b** via Oxidative Cyclization–Polymerization)*: A solution of **1b** (240 mg, 0.481 mmol) in CH_2Cl_2 (100 mL) was stirred vigorously under argon as a suspension of $FeCl_3$ (600 mg, 3.70 mmol) in CH_2Cl_2 (8 mL) under argon was added dropwise over 10 min. The solution was stirred under an argon purge for 3.5 h at which point methanol was added. After stirring for approx. 1 h, the solvents were removed under reduced pressure and the crude solids were redissolved in CH_2Cl_2. The organic phase was washed with NH_4OH (×2) and NaCl (aq), dried ($MgSO_4$) and removed in vacuo to provide the material as a dark burgandy red solid (208 mg).

*Representative Procedure from **3** via Pd Catalyzed Polymerization*: A 25 mL screw cap tube was charged with $Pd(PPh_3)_4$ (5 mg, 4.3 μmol) and **3** (74 mg, 98 μmol) and purged gently with argon. To a tared vial containing degassed toluene (1.5 mL) and DMF (0.5 mL) was added $Me_3SnSnMe_3$ (43 mg, 131 μmol), and this solution was added to the screw cap tube. [CAUTION: $Me_3SnSnMe_3$ is highly toxic and readily absorbed through the skin!] After brief argon purging and sealing of the tube, the system was heated to 90 °C for 4 days at which point the reaction mixture was added dropwise to methanol. The precipitates were filtered to provide poly(**2**) as a burgundy red solid.

*Oligo(**2**) Characerization: Dimer*: ^{1}H NMR (400 MHz, $CDCl_3$) δ: 8.06 (s, 2H), 7.89 (d, 2H, J = 5.43 Hz), 7.663 (s, 2H), 7.658 (s, 2H), 7.50 (d, 2H, J = 5.32 Hz), 4.14 (m, 4H), 4.09 (m, 4H), 1.90 (m, 4H), 1.3–1.7 (bm, 32H), 1.04 (m, 6H), 0.96 (m, 6H), 0.88 (m, 12H). ^{13}C NMR (100 MHz, $CDCl_3$) δ: 149.47, 149.43, 134.96, 134.57, 134.51, 129.73, 129.66, 123.78 (CH), 122.87, 122.83 (CH), 122.41, 119.56 (CH), 106.28 (CH), 105.99 (CH), 71.63, 71.58, 39.90, 39.77, 30.9, 29.51, 29.44, 24.2, 23.38, 23.35, 14.42, 14.37, 11.60, 11.54. HR-MS (fast atom bombardment, FAB): found m/z = 990.4812 ± 0.0030 (M^+); calc. for $C_{60}H_{78}O_4S_4$: 990.4783. Trimer: ^{1}H NMR (400 MHz, $CDCl_3$) δ: 7.99 (s, 2H), 7.96 (s, 2H), 7.83 (d, 2H, J = 5.38 Hz), 7.61 (s, 2H), 7.59 (s, 4H), 7.46 (d, 2H, J = 5.29 Hz), 4.12 (bm, 8H), 4.06 (bm, 4H), 1.92 (m, 6H), 1.2–1.8 (bm, 48H), 0.95–1.05 (m, 36H). MS (matrix-assisted laser desorption ionization, MALDI): found m/z = 1484.5768 [(M+H)$^+$]; calc. For $C_{90}H_{116}O_6S_6$+H: 1485.7181.

Received: June 20, 2001
Final version: July 30, 2001

[1] *Handbook of Conducting Polymers*, 2nd ed. (Eds: T. A. Skotheim, R. L. Elsenbaumer, J. R. Reynolds), Marcel Dekker, New York **1998**.
[2] J. Roncali, *Chem. Rev.* **1997**, *97*, 173.
[3] J. D. Debad, A. J. Bard, *J. Am. Chem. Soc.* **1998**, *120*, 2476.
[4] Neidlein prepared a similar series of 4,5,6,7-tetrasubstituted naphtho[2,1-*b*:3,4-*b*′]dithiophenes but reported no electrochemical studies: U. Dahlmann, R. Neidlein, *Helv. Chim. Acta* **1997**, *80*, 111. Kalaji and Murphy described the syntheses and attempted electropolymerizations of pendant β-thienyl tetrathiavulvalene (TTF) derivatives, but the oxidized TTF dication apparently prohibited polymer growth: A. Charlton, M. Kalaji, P. J. Murphy, S. Salmaso, A. E. Underhill, G. Williams, M. B. Hursthouse, K. M. A. Malik, *Synth. Met.* **1998**, *95*, 75.
[5] For high head-to-tail selectivites during polythiophene syntheses, see: a) R. D. McCullough, R. D. Lowe, *J. Chem. Soc., Chem. Commun.* **1992**, 70. b) T.-A. Chen, R. D. Rieke, *Synth. Met.* **1993**, *60*, 175.
[6] J. Billard, J. C. Dubois, N. H. Tinh, A. Zann, *Nouv. J. Chim.* **1978**, *2*, 535.
[7] For example, high organic field-effect mobilities (0.15 cm^2/V s) have been achieved with related fused thiophenes: a) J. G. Laquindanum, H. E. Katz, A. J. Lovinger, *J. Am. Chem. Soc.* **1998**, *120*, 664. b) H. Sirringhaus, R. H. Friend, C. Wang, J. Leuninger, K. Müllen, *J. Mater. Chem.* **1999**, *9*, 2095.
[8] N. Miyaura, T. Yanagi, A. Suzuki, *Synth. Commun.* **1981**, *11*, 513.
[9] D. Milstein, J. K. Stille, *J. Am. Chem. Soc.* **1979**, *101*, 4992.

  0935-9648/01/2312-1779 $ 17.50+.50/0

ADVANCED MATERIALS

[10] For a discussion of radical-radical couplings and radical cation electrophilic substitution pertinent to thiophene polymerizations, see: Y. Wei, C.-C. Chan, J. Tian, G.-W. Jang, K. F. Hsueh, *Chem. Mater.* **1991**, *3*, 888.
[11] In studies of non-polymerizable pendant thienyl monomers having blocking groups in the 5-thienyl position, we have observed single low potential chemical cyclization waves that exhibit complete irreversibility followed by single stable, reversible redox couples with peak anodic potentials slightly higher than that for the preceding chemical step. In the absence of blocking substituents at the reactive ring positions, these naphthodithiophene radical cations polymerize.
[12] For recent work employing $FeCl_3$ oxidation to effect arene–arene cyclizations in large oligophenylenes, see: F. Dötz, J. D. Brand, S. Ito, L. Gherghel, K. Müllen, *J. Am. Chem. Soc.* **2000**, *122*, 7707.
[13] J. L. Brédas, *J. Chem. Phys.* **1985**, *82*, 3808.
[14] T. R. Kelly, Q. Li, V. Bhushan, *Tetrahedron Lett.* **1990**, *31*, 161.
[15] K. Sonogashira, Y. Tohda, N. Hagihara, *Tetrahedron Lett.* **1975**, 4467.
[16] T. Sauer, G. Wegner, *Mol. Cryst. Liq. Cryst. B* **1988**, *162*, 97.
[17] W. T. Ford, L. Sumner, W. Zhu, Y. H. Chang, P.-J. Um, K. H. Choi, P. A. Heiney, N. C. Maliszewskyj, *New J. Chem.* **1994**, *18*, 495.
[18] Q. Zhou, P. J. Carroll, T. M. Swager, *J. Org. Chem.* **1994**, *59*, 1294.

Nanoscale Lateral Field-Emission Triode Operating at Atmospheric Pressure**

By *Laura Pescini*, *Armin Tilke*, *Robert H. Blick*,* *Heribert Lorenz*, *Jörg P. Kotthaus*, *Werner Eberhardt*, and *Dieter Kern*

Silicon-based transistors are state of the art amplifiers and only the true admirers of hifi electronics are still using tube based amplifiers, appreciating the clear sound these produce. Nevertheless, even vacuum tubes in monitors and television sets might soon be outperformed by field-emission devices in flat panel displays, which are also seen as the most promising challenge to liquid crystal displays (LCDs).[1] The main reasons for this are the very low operation voltages and, if silicon is used as the starting material, the low cost and the possibility to integrate the field-emitters in current silicon technology.[2] Commonly, field-emission devices machined on the 10 nm scale are limited to low pressures down to 10^{-9} mbar,[3] much like conventional electron tubes. Nevertheless, in recent work by Driskill-Smith et al.,[4] effective functioning of nanoscale field-emitters at atmospheric pressure was demonstrated.

The underlying idea for the device we fabricated is a combination of well-established silicon nanotechnology and of the principle of a triode amplifier. We show how this device functions as a classical triode on the nanometer scale and, resulting from the small dimensions, how it is operated under ambient pressure at room temperature. The gating allows to direct the electron current and amplify it locally with low power consumption. Typical operating voltages of the device are of the order of only 2 V, which makes it suitable for low-power electronics.

The material of choice for such three-dimensional nanosculpturing is silicon-on-insulator (SOI). The SOI wafers are highly n-doped by phosphorus diffusion from a solid dopant source. The silicon film has a thickness of 190 nm and the buried oxide (BOX) is around 360 nm. In transport measurements the doping level turned out to be about 5×10^{19} cm^{-3}. The triode structure is defined by high-resolution low-energy electron-beam lithography using a two-layer positive electron resist, namely poly(methylmethacrylate) (PMMA). A 30 nm aluminum film is evaporated to serve as an etch mask in the following reactive ion etching of the silicon film, which is performed using CF_4. Undercutting of the defined structures is achieved by removing the BOX in an etchant with a 49:1 volume ratio of H_2O/HF (water and hydrofluoric acid). The aluminum layer itself is simultaneously removed by the HF solution. Since the silicon is highly doped, this etching process also leads to an effective shrinking of the electrodes with an etch rate of about 1.8 nm/min.[5] After removing the sacrificial layer, the triodes are finally suspended in a critical point dryer in order to avoid lift-off of the triode structure by the surface tension of the solvents. The suspended silicon nanostructure is shown in Figure 1.

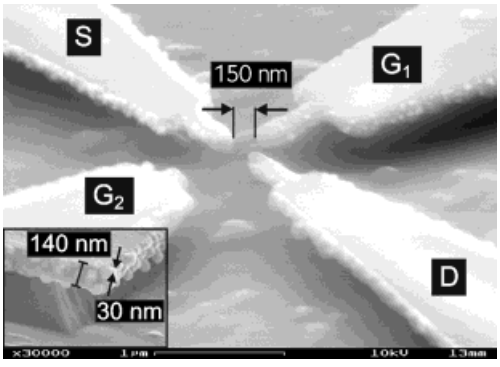

Fig. 1. Scanning electron micrograph of the free-standing silicon nanostructure: Aerial view of the device with the contacts marked as source (S), drain (D), gate 1 (G_1), and gate 2 (G_2). Inset: Silicon/phosphorus grains with sizes on the order of 10–30 nm are found on the edges of the doped substrate, constituting the field-emission tips.

We use a typical current measurement setup with low-noise preamplifiers and common voltage sources. This enables monitoring of drain and gate currents simultaneously. Most of the measurements are performed in a sample holder at room temperature, allowing the flow of different coupling gases. The devices we designed are set up much like a classical triode tube amplifier, as seen in Figure 1. The leads are completely undercut, thus inhibiting current flow across the substrate. The gate electrodes are aligned perpendicularly to source (S) and drain (D) contacts. This convention is adopted for the

[*] Dr. R. H. Blick, L. Pescini, Dr. A. Tilke, Dr. H. Lorenz, Prof. J. P. Kotthaus
Center for NanoScience and Sektion Physik
Ludwig-Maximilians-Universität
Geschwister-Scholl-Platz 1, D-80539 München (Germany)
E-mail: robert.blick@physik.uni-muenchen.de
Dr. W. Eberhardt, Prof. D. Kern
Institut für Angewandte Physik, Universität Tübingen
Auf der Morgenstelle 10, D-72076 Tübingen (Germany)

[**] We acknowledge technical support by A. Kriele and S. Manus. The SOI-wafers were donated by Siemens AG, Munich. We acknowledge financial support from the German ministry of science (BMBF) under contract number 01M2413C6 and the Deutsche Forschungsgemeinschaft (project: Bl/487–2).

  0935-9648/01/2312-1780 $ 17.50+.50/0